LASER INTERFEROMETER GRAVITATIONAL WAVE OBSERVATORY
-LIGO-
CALIFORNIA INSTITUTE OF TECHNOLOGY
MASSACHUSETTS INSTITUTE OF TECHNOLOGY

Publication LIGO-P020029- 00- D 10/30/02

An Introduction to Signal Extraction in Interferometric Gravitational-Wave Detectors

Eric D. Black and Ryan N. Gutenkunst

This is an internal working note
of the LIGO Project.

California Institute of Technology
LIGO Project - MS 51-33
Pasadena CA 91125
Phone (626) 395-2129
Fax (626) 304-9834
E-mail: info@ligo.caltech.edu

Massachusetts Institute of Technology
LIGO Project - MS 20B-145
Cambridge, MA 01239
Phone (617) 253-4824
Fax (617) 253-7014
E-mail: info@ligo.mit.edu

WWW: http://www.ligo.caltech.edu/

file http://www.ligo.caltech.edu/~ blacke/P020029-00.pdf- printed November 22, 2002

An Introduction to Signal Extraction in Interferometric Gravitational-Wave Detectors

Eric D. Black and Ryan N. Gutenkunst

LIGO Project, California Institute of Technology

Mail Code 264-33, Pasadena CA, 91125

(Dated: July 22, 2002)

Abstract

In the very near future gravitational-wave astronomy is expected to become a reality, giving us a completely new tool for exploring the universe around us. This paper provides an introduction to how interferometric gravitational-wave detectors work, suitable for students entering the field and teachers who wish to cover the subject matter in an advanced undergraduate or beginning graduate-level course.

PACS numbers: 01.30.Rr,04.80.Nn,95.55.Ym,07.60.-j

It would have been hard to imagine the wonders that would later be revealed when Karl Jansky identified the first astronomical source of radio waves [1]. Since that first, astonishing discovery, astronomers have shown us views of the universe through a wide range of the electromagnetic spectrum. This new vision has revealed to us wonders such as x-ray sources (black-hole candidates; see for example [2]), the cosmic microwave background (a relic of the birth of the universe, *e.g.* [3, 4]), and gamma-ray bursts (unknown origin [5]). Not only have we explored vast regions of the electromagnetic spectrum, we have probed neutrinos from a supernova to learn about stellar collapse [6] and from the sun to learn fundamental physics [7]. As our ability to detect different kinds of signals expands, so does our understanding of the universe around us. It is perhaps natural, then, to ask if there are other windows on the universe waiting to be discovered.

Gravitational waves may provide us with just such a window. As their name implies, gravitational waves are propagating gravitational fields, analogous to the propagating electromagnetic fields we have so effectively probed in recent years. We know that astronomical sources of gravitational waves exist, but, as of this writing, we have yet to achieve positive detection of gravitational waves on earth. This is a field potentially rich with the promise of discovery.

There are currently a number of experiments being performed and developed around the world to try and detect gravitational waves [8–14]. Much of this effort centers around interferometric detectors, and this paper is an introduction to how these detectors work. Specifically, we will describe the optical configuration of an interferometric detector and how it converts a gravitational wave into a measurable signal. In the process, we will touch on several important topics in modern experimental physics, including nulled lock-in detection and optical Fabry-Perot cavities.

I. GRAVITATIONAL WAVES

A. Properties of gravitational waves

Before we jump into the physics of gravitational-wave detectors, let us look at some of the properties of these waves. The existence of gravitational waves is predicted by general relativity, where they arise as wave-like solutions to Einstein's (linearalized) field equations [15]. Gravitational waves are similar in many ways to electromagnetic waves, which are similarly predicted from wave-like solutions to Maxwell's equations. Both kinds of waves propagate at the speed of light; both are transverse, meaning that the forces they exert are perpendicular to the direction

of propagation; and both exhibit two orthogonal polarizations. Since an electromagnetic wave carries propagating electric and magnetic fields, it should come as no surprise that a gravitational wave carries a gravitational field. While the field in an electromagnetic wave exerts a force only on charged particles, the field in a gravitational wave exerts forces on all objects. In the case of electromagnetic waves, the direction of the force exerted on a charged particle is relatively straightforward: A linearly-polarized plane wave propagating along the z-axis will exert, on a charged particle, an oscillating force along, say, the y-axis. This force will just push the (charged) particle up and down along the y-axis. (We are neglecting the contribution of the magnetic field in this example, which is valid as long as the velocity of the charged particle remains small.) The effect of a gravitational wave on matter is a little more subtle.

Instead of simply exerting an oscillating force on an object along a fixed axis, a gravitational wave produces a force that stretches and squeezes the object along two axes, as shown in Figure 1. If a gravitational wave propagating along the z-axis encounters such an object, the object will feel a compressive force along the y-axis and simultaneously a stretching force along the x-axis. Half a period later, the force along the y-axis will have reversed sign and will be trying to stretch the object, while the x-force will be compressive. This configuration describes one polarization, known as "$+$" relative to these axes. The other polarization, denoted "$\times$," has the forces being exerted along a pair of axes rotated 45° from the "$+$" case. The spatial pattern of this force resembles the tidal force exerted on a moon as it orbits a planet, and the force exerted by a gravitational wave is commonly referred to as tidal. If we replace our target object with a collection of smaller free masses, not connected to each other, then the gravitational wave just moves those masses in the same pattern as described above: pulling them together along the y-axis and pushing them apart along the x-axis, then reversing sign in the next half period.

The spatial distribution of the force exerted by a gravitational wave is more complicated than that of an electromagnetic wave, so it is perhaps not surprising that its magnitude is more subtle as well. A gravitational wave induces a *strain* in an object. The amount of stretch or compression along the x- or y-axis is proportional to the length of the object along that axis. The larger the object, the more it stretches. Both facts, that a gravitational wave induces a strain and that that strain is in a tidal pattern, influence the design of our detector.

To be precise, a gravitational wave actually produces a perturbation in the metric of space-time, but as long as our target object is small compared with the wavelength of the gravitational wave, our tidal-forces view is equivalent [16].

B. Gravitational radiation

Similar to the way electromagnetic waves are emitted by accelerating charges, gravitational waves are emitted by accelerating masses. However, the energy emitted in the form of gravitational waves for most objects in non-relativistic interactions is quite small. This is not only due to the fundamentally weak nature of gravity, but also to the fact that mass only comes in one sign. The familiar and prominent dipole radiation of electrodynamics does not occur for gravitational radiation because it is impossible to produce an oscillating dipole moment about the center of mass in a system of interacting particles. The combination of difficulty generating gravitational waves and the weak nature of the gravitational field itself makes detectable gravitational waves quite rare.

The gravitational waves we have the best chance of detecting, and the ones that are perhaps the most interesting from an astronomer's point of view, are those produced by cataclysmic events, such as black hole collisions or Type II supernovae. Such events involve gravity in the strong-field, nonlinear regime, and the radiation emitted can carry information about what goes on under these conditions. This is new territory for physics as well as astronomy, as general relativity has so far only been studied experimentally in the weak-field limit.

C. Sources of gravitational radiation

It is generally accepted that gravitational waves exist. Not only are they predicted by a well-established theory, general relativity, we also have at least one known emitter of gravitational radiation: PSR1913+16, a binary system composed of two neutron stars, one of which is a pulsar [17]. The orbital period of this system is quite short, less than eight hours, which means that two very massive, very compact objects (the two neutron stars) are experiencing strong, regular accelerations. General relativity then predicts that this system should be losing energy in the form of gravitational radiation. As this energy is lost the two neutron stars should drift closer together, and as a result the orbital period of the system should slowly decrease. We can calculate what the orbital decay of the system should be, based on general relativity. Because one of the neutron stars is a pulsar, a fine natural clock, we can also accurately measure the orbital period and plot it as a function of time. (We can tell where the system is in its orbit by looking at the doppler shift in the pulsar's signal.)

This is exactly what Russell Hulse and Joseph Taylor did as part of an extensive study of

PSR1913+16. Over the course of years of observation, the system's slow orbital decay accurately matched the predictions of energy loss from the emission of gravitational waves [18, 19]. (Hulse and Taylor won a Nobel Prize for this work in 1993.) Although the existence of gravitational waves was considered confirmed by this indirect observation, exploiting the information they carry requires observation of the waves themselves. We do not want to observe them just to confirm their existence, we want to use them to get information about the systems that emit them.

To be observable by an earth-based detector, a gravitational-wave signal should be both strong and have a relatively high-frequency. Strong signals are easier to detect than weak ones, usually, and seismic disturbances are less likely to interfere with a measurement at high frequencies than at lower ones. The roughly 7.75 hour period of PSR1913+16 makes its gravitational radiation inaccessible to a ground-based detector, but a system with a period of 10 milliseconds or less would probably produce an observable signal in such a detector. Fortunately, the shorter the period of a binary system, the greater the acceleration involved, and hence the more energy emitted in the form of gravitational waves.

The neutron stars in a binary system, such as PSR1913+16, spiral in toward each other as they lose energy, and the period of the system decreases. The two neutron stars will get closer together over time, and speed up, until they eventually collide, merging to form a single, massive object. Just before this collision the orbital frequency can be quite high, and orbital periods of 10 ms or less are easily attainable. Moreover, the amplitude of the gravitational radiation emitted increases dramatically as this inspiral progresses. The waveform of the signal produced is expected to provide a wealth of new information on the dynamics of the merger, and that is the scientific information we are after.

Other possible sources of strong, high-frequency gravitational waves include black hole-black hole mergers and Type II Supernovae. (For a nice review of possible sources, see Chapter 3 of Saulson's book [16].) These are just a few of the expected sources of gravitational radiation. A complete review of all of the possible sources belongs in a separate article devoted entirely to that subject. The most interesting sources, of course, will be the ones we did not anticipate!

II. A MICHELSON INTERFEROMETER AS A GRAVITATIONAL WAVE DETECTOR

Most modern interferometric detectors are based on the Michelson design. Michelson interferometry is particularly well-suited for detecting gravitational waves because of the geometry of

the tidal force the waves produce. A "classic" Michelson interferometer, as shown in Figure 2, is sensitive to differential motion between the x- and y-arms, just the kind of strain produced by a gravitational wave. In this basic configuration, light enters the interferometer and is split in two by a beam splitter. The two resulting beams travel down the arms, reflect off the end mirrors, and recombine to interfere back at the beam splitter [20]. The light emitted at the observation, or *antisymmetric* port provides a measure of the difference between the lengths of the interferometer's arms. (The *symmetric* port, from which light returns to the laser, also contains information about the relative arm lengths. Conservation of energy requires that the power coming out of the symmetric and antisymmetric ports, along with any power lost in the instrument, accounts for all of the input power.)

Let's consider quantitatively the response of a simple Michelson interferometer to a gravitational wave. It is not hard to derive an expression for the electric field at the output of the interferometer, E_{out}, as a function of the electric field at its input, E_{in}.

$$E_{out} = \frac{1}{2}\left(r_x\, e^{i\,k\,2\ell_x} - r_y\, e^{i\,k\,2\ell_y}\right) E_{in}. \tag{1}$$

Here ℓ_x and ℓ_y are the lengths of the two arms, k is the wavenumber for the light we are using, and r_x and r_y are the amplitude reflectivities of the end mirrors. In our convention, a perfectly reflecting mirror has $r = -1$.

The power falling on the photodiode in Figure 2 is just the square of the magnitude of the electric field, $|E_{out}|^2$, or, for perfectly reflecting end mirrors,

$$P_{out} = P_{in} \cos^2\left[k\left(\ell_x - \ell_y\right)\right],$$

where $P_{in} = |E_{in}|^2$ is the power entering the interferometer, provided by the laser in Figure 2. This output power, and hence the voltage produced by the photodiode, varies sinusoidally with the difference in arm lengths, as shown in Figure 3.

If we set the arm lengths in the absence of a gravitational wave to be ℓ_x and ℓ_y, then we can write the total arm length as $\ell_x + \delta\ell_x$ and $\ell_y + \delta\ell_y$, where a gravitational wave induces the perturbations $\delta\ell_x$ and $\delta\ell_y$. If we write the strain induced by the gravitational wave as

$$h \equiv \frac{\delta\ell_x - \delta\ell_y}{\ell},$$

then we can write the power at the output of the interferometer as

$$P_{out} = P_{in} \cos^2\left[k\left(\Delta\ell + \ell h\right)\right],$$

where $\Delta\ell = \ell_x - \ell_y$ is the asymmetry in the arm lengths that we set in the absence of a signal, and the average arm length is $\ell = (\ell_x + \ell_y)/2$.

Throughout this paper we will assume that the gravitational wave strain is very small. In this case we will assume that it its small enough that $k\ell h \ll 1$. We can then choose an *operating point* at some $\Delta\ell$ and then look at the small perturbations in the output power around that point that the gravitational wave produces. We can describe this mathematically by a Taylor expansion about $\Delta\ell$.

$$P_{out} = P_{in}\cos^2\left[k\Delta\ell\right] + P_{in}\,\frac{\partial}{\partial u}\cos^2 u\bigg|_{u=k\Delta\ell}(k\ell h) + \cdots$$

The response of our simple Michelson interferometer to a gravitational wave strain h is proportional to the derivative of the output power with respect to $\Delta\ell$, so the obvious thing to do is to operate at the point where that derivative is maximum, point 1 in Figure 3. At this point $k\Delta\ell = \pi/4$, and

$$P_{out} \approx \frac{P_{in}}{2}\left[1 - 2k\ell h\right].$$

Unfortunately, this leaves us with a fairly large dc term, $P_{in}\cos^2\left[k\Delta\ell\right] = P_{in}/2$ in this case, which will fluctuate if $\Delta\ell$ varies due to any perturbations on the mirrors, whether it be a gravitational wave, seismic disturbance, etc. More important, this dc term is proportional to P_{in}, which can fluctuate even if the mirrors remain still.

Measuring small changes in a large signal is seldom an effective way to do experimental physics. If the amplitude of the gravitational wave we want to study is very small, as is too often the case, fluctuations in the dc term described above can completely obscure our signal. What we need is a way to reduce or even eliminate the dc term while retaining and, if possible, boosting our signal. How we meet these two goals is the subject of this paper.

III. TURNING A MICHELSON INTERFEROMETER INTO A PRACTICAL GRAVITATIONAL-WAVE DETECTOR

There are four things we need to do to our simple Michelson interferometer to make it an effective gravitational-wave detector.

1. *Make it big:* Because a gravitational wave induces a strain ($\delta\ell/\ell$) between two free masses, the total distance each end mirror moves ($\delta\ell$) will be proportional to the arm length (ℓ). The longest practical arm lengths for ground-based detectors are on the order of a few kilometers.

We will show later that by *folding* the interferometer, we can squeeze effective arm lengths of several hundred kilometers or more into just a few kilometers.

2. *Use a lot of laser power:* Not surprisingly, the brighter the light source we use, the stronger our output signal will be. However, there is one additional benefit to using a lot of laser power that may not be obvious at first glance. The effects of shot noise are reduced as the laser power is increased. Using a very powerful laser for a light source is one obvious way to increase the power used, but there are clever tricks that we can use to increase the power going into the instrument even more. One such technique that is commonly used is *power recycling*, a scheme by which any unused light exiting the symmetric port (*i.e.* going back to the laser instead of falling on the photodiode) is recycled back into the interferometer. In this paper we will discuss both power recycling and the effect of shot noise on the output of an interferometric gravitational wave detector.

3. *Decouple external noise sources:* Some noise sources, such as seismic noise, act directly on the mirrors and thus compete directly with gravitational waves to produce an output signal. Other noise sources do not perturb the mirrors directly and can be thought of as "external" to the instrument. A cleverly designed interferometer can be made largely insensitive to a wide variety of these external noise sources, and in this paper we will look at one technique that is widely used in many areas of experimental physics: nulled lock-in detection. We will show how nulled lock-in detection is implemented in an interferometric gravitational-wave detector to decouple its output from fluctuations in the input power P_{in}.

4. *Reduce the noise in the mirrors:* The largest strain we expect to observe from a gravitational wave is on the order of 10^{-21} [16], which gives a mirror motion of 4×10^{-18} meters in a detector with $4\,$km arms. Obviously we must reduce the level of ambient noise in the mirrors to a level comparable to or smaller than this, at the frequencies where we expect to observe. We will not go into physical noise reduction techniques here, except to note that the whole interferometer must be enclosed in vacuum and mounted on a high-performance seismic-isolation system. As of this writing, noise reduction is a field of active and ongoing research.

Making the interferometer large and using a lot of power enhances our signal, while decoupling external noise sources eliminates the dc term we found problematic in the last section. In this paper

we will only consider these three items. A treatment of reducing the noise intrinsic to the mirrors is beyond the scope of this article, and for a nice introduction to that subject see Peter Saulson's textbook [16].

IV. DECOUPLING INTENSITY NOISE: NULLED LOCK-IN DETECTION

A. Null-point operation

To eliminate the dc term in the output, interferometers for gravitational-wave detection operate at the point labeled 2 in Figure 3, known as the *null point*. Arm lengths are chosen so that, after passing back through the beamsplitter, the two beams are 180° out of phase at the output (asymmetric) port. In the absence of a gravitational wave they interfere perfectly destructively, and no light falls upon the photo-detector; the port is "dark," even if the power delivered by the laser fluctuates.

The electric field at the output of a Michelson interferometer is given by Equation 1. Operated on a dark fringe this becomes

$$E_{out} = -iE_{in}e^{ik(\ell_x+\ell_y)}\sin\left[k\ell h\right], \tag{2}$$

where we have assumed $r_x = r_y = -1$. At this point, let us introduce a graphical method of visualizing the calculation of the output of an interferometer. Since we are using complex numbers to represent electric fields, we may plot these numbers as vectors in the complex plane, as in Figure 4. (This approach will be familiar to anyone who has studied phasors.) When we write the electric field in a light beam as $Ee^{i\omega t}$, we separate the time and spatial components of the phase into $e^{i\omega t}$ and E, respectively. In Figure 4, we plot the real and imaginary parts of the spatial component E, as a function of some position along the beam. As we advance along the beam, the spatial phase advances, and for each wavelength λ we travel, the vector representing E sweeps around full circle in the complex plane.

We can represent the calculation of the interferometer output graphically, as in Figure 5. Here, we sketch the spatial components of the phase of the beam just before the light strikes the beamsplitter the first time, where E is purely real, and after returning from each arm, where the differential motion of the end mirrors has introduced a small phase in E. This phase is positive for the y-arm (the arm along the y-axis) but negative for the x-arm because the mirrors move in opposite directions under the influence of the gravitational wave. When it reflects off of the beamsplitter,

the light from the x-arm acquires a 180° phase shift, so that when it combines with the light from the y-arm, destructive interference occurs and, in the absence of a gravitational wave, the port is dark. In the presence of a gravitational wave, the small imaginary components acquired in the x- and y-arms add constructively after the beamsplitter, resulting in a small, purely imaginary E. That this field is 90° out of phase with the light incident on the beamsplitter will be important later, when we talk about lock-in detection.

The power falling on the photodetector is just the square of the amplitude of this small, imaginary E, just after the photodetector.

$$\begin{aligned} P_{out} &= P_{in} \sin^2 [k\ell h] \\ &\approx P_{in} k^2 \ell^2 h^2, \end{aligned}$$

which is proportional to the square of the strain, h^2. We expect h to be very small, on the order of 10^{-21} or less, so an output proportional to h^2, rather than h, would be quite small and very difficult to detect. (For a kilometer-scale interferometer, P_{in} would have to be on the order of a kilowatt to produce more than one photon per second in P_{out}!) Operating at the null point has eliminated our intensity noise, but it has also nearly killed our signal! Fortunately, there is a way to recover the signal without coupling to intensity noise, and that is the subject of the next section.

B. Obtaining a Linear Signal: Lock-In Detection

We can recover a signal that is linear in h without reintroducing intensity noise by using lock-in detection [21]. In lock-in detection, we modulate the signal and observe the resulting change in the output of the instrument. We then compare that change with our modulation signal to measure the derivative of the instrument's output with respect to a signal. At the null point both the output power and its derivative are zero, but while a gravitational wave produces a second-order change in the output power, it produces a first-order change in its derivative. This first-order signal is something we have a chance of detecting.

1. Sidebands

Lock-in detection requires that we modulate the signal. The most obvious way to do that would be to purposefully move the mirrors in a way that mimics a gravitational-wave signal. In practice,

however, it is easier to both implement and describe this modulation by acting on the phase of the laser using a Pockels cell. A Pockels cell is essentially just a block of dielectric material with an index of refraction that depends on an applied electric field. If we pass the incident beam through a Pockels cell and apply an oscillating electric field to it, we will modulate the phase of the light going into the interferometer, as shown in Figure 6. The electric field of the light going into the interferometer can then be written as

$$\begin{aligned} E_{in} &= E_0 e^{i(\omega t + \beta \sin \Omega t)} \\ &\approx E_0 \left[J_0(\beta) e^{i\omega t} + J_1(\beta) e^{i(\omega+\Omega)t} - J_1(\beta) e^{i(\omega-\Omega)t} \right] \end{aligned}$$

where J_0 and J_1 are zeroth and first order Bessel functions. The first term in this equation is called the *carrier*; the next two are referred to as the *sidebands*.

We can calculate the electric field exiting the interferometer by considering the carrier and sidebands separately. We define the *transfer function* t of an interferometer for light of any given wavelength as the ratio of the output electric field to the incident field,

$$t \equiv \frac{E_{out}}{E_{in}},$$

where E_{out} is given by Equation 1. Our modulated beam is composed of three different wavelengths, so we can find an expression for the light exiting the interferometer by applying the appropriate transfer function to each part, *i.e.*

$$E_{out} = E_0 \left[t_c J_0(\beta) e^{i\omega t} + t_+ J_1(\beta) e^{i(\omega+\Omega)t} - t_- J_1(\beta) e^{i(\omega-\Omega)t} \right],$$

where t_c is the transfer function for the carrier, and $t_\pm$ are the transfer functions for the sidebands. We can calculate all of these transfer functions from Equation 1, and in fact we did calculate the transfer function for the carrier in the last section. The transfer functions for the sidebands can be got by the same procedure, if use for their wavenumbers

$$k_\pm = \frac{\omega \pm \Omega}{c} = 2\pi \left(\frac{1}{\lambda} \pm \frac{1}{\lambda_{mod}} \right).$$

Here λ_{mod} is the wavelength of an electromagnetic wave with frequency Ω. The transfer functions for the sidebands are then

$$t_\pm = i \sin \left[2\pi \left(\frac{\ell_x - \ell_y}{\lambda} \pm \frac{\ell_x - \ell_y}{\lambda_{mod}} \right) \right] e^{i\, k_{sb}\, (\ell_x + \ell_y)}.$$

2. Schnupp asymmetry

Now comes a really clever part. We still want the output of the interferometer to be dark for the carrier, but if it is also dark for our sidebands we still will have a second-order signal in h. If, however, we introduce a difference in the arm lengths $\Delta\ell \equiv \ell_x - \ell_y$, we can arrange for the output of the interferometer to be dark for the carrier but not dark for the sidebands. This trick is often attributed to Lise Schnupp, and the difference in arm lengths $\Delta\ell$ is known as the Schnupp asymmetry.

With the Schnupp asymmetry and $r_x = r_y = -1$, the sidebands' transfer function reduces to

$$t_\pm = \mp i \sin\left[2\pi\left(\frac{\Delta\ell}{\lambda_{mod}}\right)\right] e^{i\frac{\omega\pm\Omega}{c}(\ell_x+\ell_y)}.$$

We will neglect the change in $\Delta\ell$ produced a passing gravitational wave.

3. Output of the instrument

The total electric field of the light exiting the interferometer is then

$$\begin{aligned} E_{out} &= E_{in}e^{ik(\ell_x+\ell_y)}\left[iJ_0(\beta)2\pi\frac{\ell}{\lambda}h+\right. \\ &\quad \left. 2iJ_1(\beta)\sin\left(2\pi\frac{\Delta\ell}{\lambda_{mod}}\right)\cos\left(\Omega t+4\pi\frac{\ell}{\lambda_{mod}}\right)\right], \end{aligned} \tag{3}$$

where we have used Equation 2 to calculate t_c. The power falling on our photodiode, as shown in Figure 6, is then

$$\begin{aligned} P_{out} &= P_{in}J_0^2(\beta)4\pi^2\frac{\ell}{\lambda}^2h^2 + 2P_{in}J_1^2(\beta)\sin^2\left(2\pi\frac{\Delta\ell}{\lambda_{mod}}\right)+ \\ &\quad 2P_{in}J_1^2(\beta)\sin^2\left(2\pi\frac{\Delta\ell}{\lambda_{mod}}\right)\cos\left(2\Omega t+8\pi\frac{\ell}{\lambda_{mod}}\right)+ \\ &\quad P_{in}J_0(\beta)J_1(\beta)4\pi\frac{\ell}{\lambda}h\sin\left(2\pi\frac{\Delta\ell}{\lambda_{mod}}\right)\cos\left(\Omega t+4\pi\frac{\ell}{\lambda_{mod}}\right) \end{aligned} \tag{4}$$

The voltage the photodiode produces is linearly proportional to the power falling on it, so for our purposes the signal we measure at the photodiode will just be $V_{pd} = RP_{out}$, where R is the response of the photodiode.

There are four terms in this signal: two at dc, one oscillating at 2Ω, and one oscillating at Ω. The one oscillating at Ω is proportional to the gravitational-wave strain h and is the term we would like to isolate and measure. We isolate this term through a process standard in lock-in

detection known as *mixing*, followed by low-pass filtering, or averaging over time. Mixing just means multiplication, and a mixer is a nonlinear device that takes two voltages on its inputs and produces a voltage at its output that is proportional to the product of the voltages at its inputs. If we feed V_{pd} into one input and $V_{osc}cos(\Omega t + \phi)$ into the other, then we can write the time-averaged output of the mixer as

$$\begin{aligned} V_{signal} &= \langle V_{pd} cos(\Omega t + \phi) \rangle \\ &= 2\pi \left(RP_{in}\right) J_0(\beta) J_1(\beta) \frac{\ell}{\lambda} \sin\left(2\pi \frac{\Delta\ell}{\lambda_{mod}}\right) h, \end{aligned} \tag{5}$$

where we have adjusted the user-defined phase ϕ to maximize the signal, and we have assumed that the amplitude V_{osc} is fixed and does not contribute to changes in the output. The signal we measure is now linear in h and zero in the absence of a gravitational wave. There is no dc offset to couple fluctuations in P_{in} to the output. A graphical representation of this calculation is illustrated in Figure 7.

The sensitivity of our nulled lock-in scheme depends on the average length of the arms ℓ, the input laser power P_{in}, and the size of the Schnupp asymmetry $\Delta\ell$, all of which we would like to optimize to boost our signal. The best choice of the Schnupp asymmetry for this configuration is $\Delta\ell \approx \lambda_{mod}/4$, and this is neither difficult to achieve nor a very strict requirement. The size of the interferometer and the input power, however, should both be made as large as possible, and there are some interesting tricks for increasing both. We will consider techniques for increasing P_{in} and ℓ in the next two sections.

V. INCREASING THE ARM LENGTH: FABRY-PEROT CAVITIES IN THE ARMS

As we saw in the last section, longer arms yield larger signals. On Earth, we can't afford to build arbitrarily long arms, but we can increase the effective length of the arms by bouncing the light back and forth within them, or *folding*. Figure 8 shows a simple folding scheme for one arm of an interferometer, where an optical length of 5ℓ is folded into a physical length of only ℓ. This is conceptually the easiest folding scheme to understand, and it is the one that Michelson and Morley used in their famous experiment. However, this scheme requires a number of different mirrors, one for each fold in the optical path. A simpler scheme to implement, one that involves only two mirrors regardless of the number of folds, involves the use of a Fabry-Perot cavity [22].

A comprehensive treatment of Fabry-Perot cavities can be found in any good optics text, such

as Hecht [20] or Siegman [23]. In this analysis we are only concerned with the transfer functions of these cavities, so let us review, briefly, what we need to know to proceed. A Fabry-Perot cavity is just two parallel, partially transmitting mirrors, as shown in Figure 9. Most of the light falling on the input mirror reflects off of it, and this is referred to as the *promptly reflected* beam. Some light, however, leaks through and circulates between the input and output mirrors. If this light returns from one round trip in-phase with new light leaking in, constructive interference will occur and a standing wave will build up, a condition known as *resonance*. The amplitude of this standing wave can become quite large, much larger than the amplitude of the incident light. When this occurs, the small fraction of that light that leaks out of the input and output mirrors can become comparable, in intensity, to the incident and promptly reflected beams. When this happens, the resulting *leakage* beam will interfere with the promptly reflected beam, and some interesting things will happen.

Near resonance, the phase of this leakage beam is very sensitive to the distance between the mirrors, so a Fabry-Perot cavity can be used as a high-precision measuring device, capable of detecting very small deviations in the distance between its mirrors. If the resonance condition is not met exactly, then any small phase shift that the light picks up in one round trip will get amplified by the total number of round trips it makes before leaking back out. In this sense the standing wave is analogous to the multiple bounces in a delay line, where the number of bounces is determined by the average storage time of the cavity, *i.e.* the average number of round trips a photon makes before leaking back out. If we replace the arms of a gravitational-wave detector with long Fabry-Perot cavities, as shown in Figure 10, we can achieve folding and increase the effective arm length by a factor proportional to the storage time, or the average number of bounces, of the cavity.

Thinking of a Fabry-Perot cavity as a delay line is useful conceptually, but for a quantitative model the analogy is of limited use. We will need a quantitative model of Fabry-Perot cavities in this section and the next, so let's establish a few important properties of Fabry-Perot cavities now.

The ratio of the incident to reflected electric fields just before the input mirror is known as the reflection coefficient of the cavity, and it is easy to derive. The result is

$$r = \frac{-r_i + r_o(r_i^2 + t_i^2)e^{i\,4\pi L/\lambda}}{1 - r_i r_o e^{i\,4\pi L/\lambda}}, \tag{6}$$

where L is the length of the cavity, r_i and r_o are the amplitude reflection coefficients of the input and output mirrors, and t_i is the amplitude transmission coefficient of the input mirror. For lossless mirrors $|r|^2 + |t|^2 = 1$. Resonance occurs whenever $2L = N\lambda$, where N is an integer. How

precisely this condition must be met for resonance to occur depends on the reflectivities of the input and output mirrors. If the input mirror has a relatively high transmission coefficient, *i.e.* it lets a fairly large amount of the incident light leak into the cavity, then the condition $2L = N\lambda$ does not have to be met very precisely for resonance to occur. If the input mirror is highly reflective, then the tolerances on $2L = N\lambda$ are much tighter. A measure of how sensitive the cavity is to changes in L or λ is the *finesse* of the cavity, $\mathcal{F}$, defined as the full width at half maximum of the amplitude of the standing wave inside the cavity, or *linewidth*, divided by the spacing between resonances, or *free spectral range*. If we consider λ fixed and allow L to vary, then the finesse is given by

$$\mathcal{F} \equiv \frac{\Delta L_{lw}}{\lambda/2},$$

where ΔL_{lw} is the linewidth. Now, this linewidth depends, as we have said, on the reflectivities of the mirrors, so we may as well define the finesse in terms of these reflectivities. For any Fabry-Perot cavity, the finesse can be written [23]

$$\mathcal{F} = \frac{\pi\sqrt{r_i r_o}}{1 - r_i r_o}.$$

Now let's talk about how the reflectivities of the mirrors affect the behavior of the cavity. If we plot the reflection coefficient of a Fabry-Perot cavity in the complex plane, we find that it is always a circle [24]. The properties of this circle depend on the properties of the cavity, and there are three cases that we need to consider, $r_i = r_o$, $r_i < r_o$, and $r_i > r_o$. The reflection coefficients for each case are illustrated in Figure 11. Far from resonance, the reflection coefficient for each case is close to -1, and its phase is relatively insensitive to changes in L or λ. As we approach resonance, say by sweeping L at a constant rate, the reflection coefficient advances around the circle in the counterclockwise direction, picking up speed as it approaches the rightmost edge of the circle. On resonance, the reflection coefficient lies on the rightmost edge of the circle, and its phase is changing the most rapidly for a given change in L. After we pass through resonance, the reflection coefficient tracks along the top half of the circle and approaches -1 again, slowing down as it gets farther from resonance. It is this sensitivity in phase to changes in L near resonance that makes a Fabry-Perot cavity a useful device for measuring small changes in distance between the mirrors, and that is why we want to use it in our gravitational-wave detector.

If both mirrors are lossless and have equal reflectivities, then on resonance the net reflected beam vanishes. Sufficient power builds up inside the cavity that the leakage beam exactly cancels the promptly reflected beam, and the reflection coefficient goes to zero. All of the incident power

gets transmitted through the cavity. When this condition is met ($r_i = r_o$ and both are lossless), the cavity is referred to as *critically coupled*.

If the output mirror is much more reflective than the input mirror, and again both are lossless, then very little light gets transmitted through the cavity, even on resonance. The leakage beam (through the input mirror) has a larger amplitude than the promptly reflected beam, and there is some net reflected light even on resonance. In this case the cavity is referred to as *overcoupled*.

If the output mirror is less reflective than the input mirror, then again little light gets transmitted through the cavity on resonance. This time, however, it is the promptly reflected beam that dominates, and the phase of the net reflected light is $-180°$, as shown in Figure 11. (Note that the leakage beam is $180°$ out of phase with the promptly reflected beam on resonance, regardless of the coupling.)

If we want to use Fabry-Perot cavities as delay lines in the arms of a Michelson interferometer and recombine the light back at the beamsplitter, and especially if we want to implement power recycling, it is best for us to use a strongly over-coupled cavity. In this case essentially all of the light is reflected when the cavity is on resonance, and the phase of this reflected light is very sensitive to deviations from resonance, as shown in Figure 12.

Near resonance, the reflection coefficient for an overcoupled, lossy Fabry-Perot cavity of length L and finesse $\mathcal{F}_{ac}$ is approximately

$$r_{x,y} = \left(1 - \frac{1}{\pi}\mathcal{F}_{ac}\epsilon\right)\left[1 + i8\mathcal{F}_{ac}\frac{\delta L_{x,y}}{\lambda}\right], \tag{7}$$

where $\delta L_{x,y}$ represents a small length deviation in either the x- or y-arm from perfect resonance, and we have approximated the finesse of an overcoupled cavity by

$$\mathcal{F}_{ac} \approx \frac{2\pi}{t_i^2}.$$

The parameter ϵ is the fractional power lost in one round trip inside the cavity, which is typically small but not negligible for a 4 kilometer Fabry-Perot cavity. For the arm cavity to be overcoupled this loss must be less than the transmission of the arm cavity's input mirror, and in all our approximations for the arm cavities we will assume this to be the case.

We may use this reflection coefficient in place of the ordinary mirror reflection coefficients $r_{x,y}$ in Equation 1 to find the transfer function of an interferometer with Fabry-Perot cavities in its arms. Only the carrier needs to resonate in the arm cavities. We will assume that the sidebands reflect off the arm cavities' input mirrors, and we will use a reflection coefficient of $r_{x,y} = -1$ for

them. The Schnupp asymmetry then only needs to be introduced between the beamsplitter and the arm cavities' input masses, and these distances can be only a few meters, as opposed to several kilometers between the mirrors that form the Fabry-Perot cavities in the arms. From now on we will use a lower-case $\ell_{x,y}$ to refer to the distance between the beamsplitter and the first, or input, mirror in the x- and y-arms. We will use an upper case $L_{x,y}$ to refer to the lengths of the Fabry-Perot cavities in the arms. Assuming that both arm cavities have the same length L in the absence of a gravitational wave and that $\ell_{x,y} \ll L$, we can get the transfer functions of an interferometer with Fabry-Perot cavity arms for both the carrier and the sidebands by combining Equations 1 and 7. They are, approximately,

$$t_c^{ifo} = i4e^{ik(\ell_x+\ell_y)}\mathcal{F}_{ac}\frac{L}{\lambda}\left(1-\frac{1}{\pi}\mathcal{F}_{ac}\epsilon\right)h,$$

and

$$t_\pm^{ifo} = \mp ie^{ik_\pm(\ell_x+\ell_y)}\sin\left(2\pi\frac{\Delta\ell}{\lambda}\right).$$

These transfer functions yield a demodulated signal of

$$V_{signal} = 4\left(RP_{in}\right)J_0(\beta)J_1(\beta)\mathcal{F}_{ac}\frac{L}{\lambda}\sin\left(2\pi\frac{\Delta\ell}{\lambda_{mod}}\right)\left(1-\frac{1}{\pi}\mathcal{F}_{ac}\epsilon\right)h, \tag{8}$$

where we have again optimized the phase ϕ in the mixing process to maximize our signal. The introduction of folding using Fabry-Perot cavities in the arms has increased the effective length of the arms by about a factor of $\mathcal{F}_{ac}$, with a corresponding increase in the strength of the readout signal. A representative value of the finesse of an arm cavity in a real detector is $\mathcal{F}_{ac} \approx 130$ [25].

VI. BOOSTING THE EFFECTIVE POWER: POWER RECYCLING

We have seen how folding increases the effective length L of an interferometer without the need to make the instrument physically larger. Now we will turn to the input power P_{in} and see how that can be boosted, with a corresponding boost in the response of the instrument.

The most obvious solution is to use a stronger light source. As of this writing, most gravitational-wave detectors use lasers that operate on the order of $10W$, and $100W$ lasers are in development. However, in a process similar to folding, we can increase the effective power going into the instrument without changing the power of the laser. How is this possible? Well, if the output port is dark, energy conservation demands that the majority of the light gets reflected back towards the laser. If we could somehow recycle this wasted light and send it back into the

interferometer, we could boost the sensitivity of the instrument without having to develop a more powerful laser. (And we could get even more out of such a laser when it becomes available.)

We saw in the last section how a Fabry-Perot cavity could be used to implement folding of an optical path. A similar concept can also be used to implement power recycling [26]. In this case, we place a single, partially transmitting mirror between the laser and the beamsplitter in our gravitational-wave detector. The interferometer itself, the beamsplitter and arms, acts like a partially transmitting mirror. Some of the light incident on the beamsplitter gets transmitted through the instrument, coming out the dark port, while most of it (most of the carrier, anyway) gets reflected back towards the laser. If we think of the interferometer just as a compound mirror, then we can use it as the output mirror of a Fabry-Perot cavity, placing a second, ordinary mirror between it and the laser. This second mirror then acts as the input mirror, and if we control the distance between it and the interferometer (the compound output mirror), then we can build up a standing wave between the two, effectively increasing the power incident on the interferometer by a factor proportional to the finesse of the resulting cavity. We will refer to this cavity as the *recycling cavity*, and we refer to the mirror we have introduced between the laser and the beamsplitter as the *recycling mirror*.

The transmission coefficient of the complete interferometer, including power recycling and Fabry-Perot cavities in the arms, is just the transmission coefficient of the recycling cavity, with the recycling mirror forming the input mirror and the rest of the interferometer acting as the output mirror. The recycling cavity reflection coefficient is just given by Equation 6, with the transmission and reflection coefficients of the compound mirror, the interferometer with Fabry-Perot arm cavities, substituted for the output mirror coefficients t_o and r_o. The transmission coefficient of the recycling cavity is the same as that for any Fabry-Perot cavity, or

$$t_{rc} = \frac{t_{rm} t_{ifo} e^{i2\pi \ell_{rm-bs}/\lambda}}{1 - r_{rm} r_{ifo} e^{i4\pi \ell_{rm-bs}/\lambda}}, \tag{9}$$

where t_{rm} and r_{rm} are the transmission and reflection coefficients for the recycling mirror, t_{ifo} and r_{ifo} are the transmission and reflection coefficients for the rest of the interferometer, and ℓ_{rm-bs} is the distance from the recycling mirror to the beamsplitter. Another way to think of ℓ_{rm-bs} is the distance between the input and (compound) output mirrors in the recycling cavity.

We calculated the transmission coefficients t_{ifo} for the carrier and sidebands in Section V. The reflection coefficients are calculated in a similar manner.

$$r_{ifo} = \frac{1}{2} e^{ik(\ell_x + \ell_y)} \left[r_x e^{ik(\ell_x - \ell_y)} + r_y e^{-ik(\ell_x - \ell_y)} \right] \tag{10}$$

Here, as before, ℓ_x is the distance from the beamsplitter to the first mirror in the x-arm (the input mirror to the x-arm's Fabry-Perot cavity), and ℓ_y is the distance from the beamsplitter to the y-arm's input mirror.

A. Sidebands

For the sidebands, which do not resonate in the arm cavities, the reflection coefficients are

$$r_x = r_y = -1$$

This yields

$$r_\pm^{ifo} = -e^{ik_\pm(\ell_x+\ell_y)} \cos\left(2\pi\frac{\Delta\ell}{\lambda_{mod}}\right)$$

and

$$t_\pm^{ifo} = \mp ie^{ik_\pm(\ell_x+\ell_y)} \sin\left(2\pi\frac{\Delta\ell}{\lambda_{mod}}\right).$$

Plugging these into our expression for r_{rc}, we find that the resonance condition is now

$$e^{ik_\pm(2\ell_{rm-bs}+\ell_x+\ell_y)} = -1,$$

and critical coupling, *i.e.* optimum recycling, requires that we adjust the Schnupp asymmetry so that

$$\cos\left(2\pi\frac{\Delta\ell}{\lambda_{mod}}\right) = r_{rm}.$$

With these conditions, the transmission coefficients for the sidebands through the recycling cavity (the complete interferometer) are

$$t_\pm^{rc} = \pm ie^{-ik_\pm\ell_{rm-bs}}.$$

The full power of the sidebands gets transmitted, and the field picks up a phase factor.

B. Carrier

We can calculate the transmission and reflection coefficients of the compound mirror for the carrier the same way we calculated them for the sidebands. Using the reflection coefficients $r_{x,y}$ from an overcoupled Fabry-Perot cavity near resonance, we find

$$t_c^{ifo} = ie^{ik(\ell_x+\ell_y)} 4\mathcal{F}_{ac}\frac{L}{\lambda}h\left(1-\frac{1}{\pi}\mathcal{F}_{ac}\epsilon\right)$$

and

$$r_c^{ifo} = e^{ik(\ell_x+\ell_y)}\left(1 - \frac{1}{\pi}\mathcal{F}_{ac}\epsilon\right).$$

Using these to find the carrier transmission and reflection coefficients for the recycling cavity, we find that the resonance condition is

$$e^{ik(2\ell_{rm-bs}+\ell_x+\ell_y)} = 1,$$

and the requirement for critical coupling is

$$r_{rm} = \left(1 - \frac{1}{\pi}\mathcal{F}_{ac}\epsilon\right).$$

The requirements for resonance and critical coupling for both the carrier and the sidebands can be combined. They are

$$\cos\left(2\pi\frac{\Delta\ell}{\lambda_{mod}}\right) = r_{rm} = \left(1 - \frac{1}{\pi}\mathcal{F}_{ac}\epsilon\right),$$
$$e^{ik(2\ell_{rm-bs}+\ell_x+\ell_y)} = 1,$$

and

$$e^{ik_{mod}(2\ell_{rm-bs}+\ell_x+\ell_y)} = -1.$$

The Schnupp asymmetry and the reflectance of the recycling mirror must both be adjusted to match the product of the arm cavities' loss and finesse, and the effective length of the recycling cavity becomes the sum of ℓ_{rm-bs} and the average length $(\ell_x + \ell_y)/2$. This effective length must be both a multiple of $\lambda/2$, where λ is the wavelength of the light used in the interferometer, and a multiple of $\lambda_{mod}/4$, where the modulation wavelength is given by λ_{mod}. The first condition tells us that the carrier must be resonant in the recycling cavity. Because the second condition is $\lambda_{mod}/4 = \ell_{rm-bs} + (\ell_x + \ell_y)/2$, we say that the sidebands must be anti-resonant in the recycling cavity. Since $\lambda \approx 1\mu m$ and $\lambda_{mod} \approx 30m$, it is not hard to achieve both of these conditions at the same time.

With both the carrier and sidebands resonating in the recycling cavity and critically coupled (optimally recycled), the transfer function for the carrier through the recycling cavity (*i.e.* the complete interferometer) becomes

$$t_c^{rc} = ie^{-ik\ell_{rm-bs}}\frac{4}{\sqrt{\pi}}\mathcal{F}_{ac}\sqrt{\mathcal{F}_{rc}}\frac{L}{\lambda}h,$$

where we have approximated the finesse of the optimally-coupled recycling cavity as

$$\mathcal{F}_{rc} \approx \frac{\pi}{t_i^2}.$$

C. DC response of the interferometer

We are now in a position to calculate the response of the complete interferometer, including lock-in detection, Fabry-Perot arm cavities, and power recycling. All we need to do is calculate the electric field of the light falling on the photodiode,

$$E_{out} = E_{in}\left[t_c^{rc}J_0(\beta)e^{i\omega t} + t_+^{rc}J_1(\beta)e^{i(\omega+\Omega)t} - t_-^{rc}J_1(\beta)e^{i(\omega-\Omega)t}\right],$$

then demodulate and average the resulting power.

$$V_{signal} = R\langle|E_{out}|^2\cos(\Omega t+\phi)\rangle,$$

where the angled brackets $\langle$ and $\rangle$ denote time averaging. The result is

$$V_{signal} = \frac{4}{\sqrt{\pi}}\left(RP_{in}\right)J_0(\beta)J_1(\beta)\mathcal{F}_{ac}\sqrt{\mathcal{F}_{rc}}\frac{L}{\lambda}h \tag{11}$$

Note that the response of the interferometer is enhanced by $\sqrt{\mathcal{F}_{rc}}$, a relatively minor improvement compared with the $\mathcal{F}_{ac}$ gain from using Fabry-Perot cavities as delay lines in the arms. A moment's thought shows that this should not surprise us. The response of the basic interferometer, given in Equation 5, is proportional to the electric ***field*** in the carrier, $\sqrt{P_{in}}J_0(\beta)$, multiplied by the ***field*** in the sidebands, $\sqrt{P_{in}}J_1(\beta)$, multiplied by the length of the arms, ℓ. Folding the arms using Fabry-Perot cavities increases the effective length to $(2/\pi)\mathcal{F}_{ac}\ell$ because the total number of round trips in a Fabry-Perot cavity is proportional to its finesse. The field in a cavity, however, is proportional to the square root of its finesse. Since the sidebands do not resonate in the arm cavities, only the carrier field is boosted by power recycling. The response of the instrument then is enhanced by the new field amplitude in the carrier, or

$$E_{carrier} \propto \sqrt{\mathcal{F}_{ac}}\sqrt{P_{in}}J_0(\beta).$$

D. AC response of the interferometer

So far we have performed all of our calculations under the assumption that the interferometer is in a quasi-static state. We have not taken into account dynamic effects. As long as any change in the instrument occurs on a time scale longer than the time it takes light to propagate completely through the instrument, this assumption is valid. However, if our gravitational-wave signal h includes components at high enough frequencies, we cannot expect our quasi-static version of the

response of the instrument to be valid. Before addressing the dynamic response of the interferometer, let us consider what these relevant time scales are, and what exactly "high frequency" means.

How long does it take for the light in the interferometer to come to a steady state? Put another way, how long does it take for an appreciable field to build up inside a Fabry-Perot cavity so that the appropriate interference can occur? Light makes a single round trip inside a cavity in a time $2L/c$, and if we think of the finesse as a measure of the total number of round trips the light makes, then the relevant time scale for equilibrium in a Fabry-Perot cavity must be approximately

$$\tau \sim \frac{2L}{c}\mathcal{F}.$$

Any signals at frequencies of $f_0 \ll 1/\tau$ will satisfy the quasi-static requirement, but frequencies on the order of or greater than $1/\tau$ will be high enough to begin to probe the dynamic response of the interferometer.

If the arm cavities have finesses of 130 and lengths of 4 kilometers, the characteristic frequency is

$$\frac{1}{\tau} \sim 300Hz,$$

which is low enough to be a problem if we are looking for signals at frequencies up to a kilohertz. The recycling cavity, on the other hand, also has $\mathcal{F}_{rc} \approx 100$, but its length is on the order of 10 meters, giving it a cutoff frequency closer to $100kHz$. Our rough estimate shows that, for searching for gravitational waves at frequencies above a few hundred hertz, we must take into account the storage time τ of the arm cavities, but not that of the recycling cavity.

A careful derivation shows that the finite storage time of the arm cavities introduces a single pole in the response of the interferometer, and that the cutoff frequency f_0 is actually $1/2\tau$, or [27]

$$f_0 = \frac{c}{4L\mathcal{F}_{ac}}.$$

The dynamic response of the interferometer to a gravitational wave signal $h(f)$ at frequency f has the same frequency-dependence as a simple, single-pole low-pass filter. For frequencies well below the recycling cavity's cutoff frequency this is [25],

$$V_{signal}(f) = \frac{4}{\sqrt{\pi}}\left(RP_{in}\right) J_0(\beta)J_1(\beta)\mathcal{F}_{ac}\sqrt{\mathcal{F}_{rc}}\frac{L}{\lambda}\frac{f_0}{f_0 + if}h(f). \tag{12}$$

VII. SHOT NOISE

No treatment of gravitational-wave detectors would be complete without some consideration of noise. Even in a $4km$ instrument, a strain of 10^{-21} produces motions of the end mirrors on the order of 10^{-18} meters, or one thousandth of the diameter of an atomic nucleus. Any instrument capable of detecting such motion must have a very low intrinsic noise level! The extraordinary sensitivity required for gravitational-wave astronomy demands that our instrument have an extremely low noise floor, and to accomplish that we must have an understanding of the physics behind the noise. There are three principal sources of noise in an interferometric gravitational-wave detector. They are

1. *Seismic Noise:* If the ground shakes, that will perturb our mirrors and can mimic a gravitational-wave strain h.

2. *Thermal Noise:* Motion of the individual molecules in the mirrors and suspensions due to heat.

3. *Shot Noise:* Optical readout noise in our photodetector.

The first two, seismic and thermal noise, can be reduced by clever design of the tables and suspensions used to hold the mirrors, and by an appropriate choice of the mirror material and geometry. The third, shot noise, is a fundamental consequence of the quantum nature of light.

In this section we will consider the limit that shot noise places on our ability to detect a gravitational-wave strain h. The rms fluctuation in the power falling on the photodiode determines the shot noise seen in the readout of the instrument. We can use the standard formula for shot noise to calculate this fluctuation.

$$\Delta P_{shot,rms} = \sqrt{2\hbar\omega P_{dc}\Delta f},$$

where P_{dc} is the average dc power falling on the photodiode, and Δf is the measurement bandwidth. It will be useful for us to express this in terms of a voltage fluctuation per unit bandwidth, or

$$V_{shot}(f) = R\sqrt{2\hbar\omega P_{dc}}.$$

We can think of this as a Fourier transform of the shot noise voltage, expressing the noise density at a given frequency, and the above expression has units of volts per square-root hertz. Note that the

amplitude of the shot noise in the photodiode does not depend on frequency, only on the bandwidth of our measurement Δf.

This shot noise appears as a signal in our readout, and we would like to know how large h has to be to stand out above the noise. All we have to do to answer this question is set the output of the instrument, Equation 12, equal to the signal due to shot noise.

$$V_{signal}(f) = V_{shot}(f),$$

or

$$\frac{4}{\sqrt{\pi}} \left(RP_{in}\right) J_0(\beta) J_1(\beta) \mathcal{F}_{ac} \sqrt{\mathcal{F}_{rc}} \frac{L}{\lambda} \sqrt{\frac{f_0^2}{f_0^2 + f^2}} \left|h_{shot}(f)\right| = \sqrt{2\hbar\omega P_{dc}} R.$$

The average dc power is simply got from the output field, as we calculated in the last section.

$$P_{out} = \langle |E_{out}|^2 \rangle = 2J_1^2(\beta) P_{in}$$

This gives us an expression for the shot noise limited sensitivity of an interferometric detector.

$$\left|h_{shot}(f)\right| = \frac{\pi}{2} \frac{\sqrt{\hbar\lambda c}}{J_0(\beta)\sqrt{P_{in}}\mathcal{F}_{ac}\sqrt{\mathcal{F}_{rc}}L} \sqrt{\frac{f_0^2 + f^2}{f_0^2}} \tag{13}$$

Note that, even though the shot noise in the photodetector itself is frequency independent, the frequency-*dependent* response of the interferometer makes the shot noise limit turn up at high frequencies. This effect is merely a result of dividing the (flat) shot noise spectrum by the response of the interferometer.

Representative parameters for a first-generation gravitational-wave detector are $L = 4km$, $\lambda = 1\mu m$, $\mathcal{F}_{ac} = 130$, $\mathcal{F}_{rc} = 100$, and $P_{in} = 10W$. This gives a dc shot noise of approximately

$$\left|h_{shot}(0)\right| \approx 10^{-23} Hz^{-1/2}.$$

VIII. OPERATING AN INTERFEROMETRIC GRAVITATIONAL-WAVE DETECTOR

Our analysis of an interferometric gravitational-wave detector has relied on resonance conditions being satisfied, which involves maintaining precise distances between mirrors over long periods of time. The systems necessary to hold the Fabry-Perot cavities in the arms on resonance, the recycling mirror at its optimum position, and to keep the output port dark for the carrier are elaborate, sophisticated, and beyond the scope of this paper. For our purposes, an analysis of signal extraction and shot noise, we can just assume that all of these conditions are met. The automatic control systems that maintain them are considered transparent for this analysis, and their inner workings are a separate study of modern experimental technique.

IX. SUGGESTED EXERCISES

1. Derive the transmission coefficients for a simple Michelson interferometer at both the symmetric and antisymmetric ports, Equations 1 and 10, respectively. There is a subtlety here that is important to appreciate before going on to do any other calculations involving interferometry: The reflection coefficient of the beamsplitter depends on the incoming direction of the incident light. In our case, we considered reflection from the left to have $r = -1/\sqrt{2}$ and from the right, $r = +1/\sqrt{2}$. This is, of course, a slight oversimplification. The mirrors in modern interferometers are made up of multilayer dielectric coatings, with complicated transmission and reflection coatings. Nevertheless, this asymmetry in the sign of the reflection coefficient, and *not* the transmission coefficient, is required for the instrument to satisfy conservation of energy. This is a general property of mirrors and is not limited to beamsplitters!

2. Derive the reflection and transmission coefficients for a Fabry-Perot cavity, Equations 6 and 9 respectively. Again, conservation of energy requires that the reflection coefficient of the input mirror have a different sign for light incident from the left than for light incident from the right. The usual derivation of these coefficients is by summing an infinite series, as in Hecht [20]. However, a much more elegant method can be found in Siegman [23].

3. *Field Lines 1:* Consider two points in space-time in the x-y plane: an origin, described by $(0, 0, 0, 0)$, and some other point $(ct, x, y, 0)$. The interval s between these two points is given, in the ordinary case of flat space-time, by

$$s^2 = -c^2t^2 + x^2 + y^2.$$

The differential interval between two points in space-time can be expressed more generally as

$$ds^2 = g_{\mu\nu}dx^\mu dx^\nu,$$

where the metric $g_{\mu\nu}$ is known as the metric tensor. (Here we employ the usual Einstein summation convention: summation over repeated indices.) For the flat space-time of special

relativity, this metric tensor is just

$$g_{\mu\nu} = \eta_{\mu\nu} = \begin{bmatrix} -1, & 0, & 0, & 0 \\ 0, & 1, & 0, & 0 \\ 0, & 0, & 1, & 0 \\ 0, & 0, & 0, & 1 \end{bmatrix}$$

We can describe a gravitational wave propagating along the z-axis, with (low) frequency $\omega/2\pi$ and "$+$" polarization, by a perturbation of this metric [15, 16].

$$g_{\mu\nu} \rightarrow \eta_{\mu\nu} + h_{\mu\nu},$$

where the additional, perturbative term is given by

$$h_{\mu\nu} = \begin{bmatrix} 0, & 0, & 0, & 0 \\ 0, & 1, & 0, & 0 \\ 0, & 0, & -1, & 0 \\ 0, & 0, & 0, & 0 \end{bmatrix} h\cos[\omega(t - z/c)]$$

This change in the metric is analogous to the movement of a free particle at coordinates x and y under the influence of a gravitational wave. Construct a vector field, at a fixed time t in the x-y plane, that describes this change in the metric and plot it.

Solution: The metric between the origin and any point in the x-y plane is given by

$$s^2 = -c^2t^2 + \left(x^2 + y^2\right) + \left(x^2 - y^2\right) h\cos(\omega t).$$

The change in the metric for a given point at coordinates x and y at time $t = 0$ is then

$$\delta s^2 = \left(x^2 - y^2\right) h.$$

The spatial gradient of this change is analogous to the pattern of motion induced.

$$\vec{g} = \vec{\nabla}\delta s^2 = 2x\hat{i} - 2y\hat{j}.$$

See Chapter 5 of Ohanian [15] for a rigorous treatment of the theory of gravitational waves.

4. *Field Lines 2:* Now consider the case of "$\times$" polarization, where the metric perturbation is given by

$$h_{\mu\nu} = \begin{bmatrix} 0, & 0, & 0, & 0 \\ 0, & 0, & 1, & 0 \\ 0, & 1, & 0, & 0 \\ 0, & 0, & 0, & 0 \end{bmatrix} h\cos[\omega(t - z/c)]$$

Again, construct and plot a vector field describing the lines of force. Show that a Michelson interferometer with arms oriented along the x- and y-axes is not sensitive to "$\times$"-polarized gravitational waves.

5. Note that the response of an interferometric gravitational-wave detector with Fabry-Perot arm cavities depends on the product of the arm length and the arm cavity finesse, $\mathcal{F}_{ac}L$. Why, then, do we need to build detectors with kilometer-scale arms? Wouldn't it be easier to keep the arm lengths at a few tens of meters (laboratory scales) and compensate by increasing the arm-cavity finesse?

   Solution: There are many answers to this question. The easiest to understand, at this level, is this: The response of the instrument, as in Equation 12, actually scales as the product $\mathcal{F}_{ac}Lh$. The amount of motion induced in the mirrors by a gravitational wave scales with the length of the instrument, Lh, whereas most external noise sources, such as seismic or thermal noise, move the mirrors by an amount that is independent of the arm length. Thus the signal-to-noise ratio of the instrument scales as the arm length L.

Acknowledgments

We would like to thank Ken Libbrecht, the Richter Memorial Fund, and the Caltech SURF program for financial support during the preparation of this paper. We are also deeply indebted to Ron Drever, for sharing his personal experience with the development of interferometric detectors, and to Stan Whitcomb, for review of the manuscript and for many interesting discussions. This work was supported by the National Science Foundation under Grant No. PHY98-01158.

---

[1] Karl G. Jansky. Electrical disturbances apparently of extraterrestrial origin. *Proc.IRE*, 21:1387, 1933.

[2] A. P. Cowley. Evidence for black holes in stellar binary systems. *Annual Reviews of Astronomy and Astrophysics*, 30:287, 1992.

[3] A. A. Penzias and R. W. Wilson. *Astrophysical Journal*, 142:419, 1965.

[4] A. H. Jaffe et al. Cosmology from MAXIMA-1, BOOMERANG, and COBE DMR cosmic microwave background observations. *Physical Review Letters*, 86(16):3475–3479, April 2001.

[5] V. Schönfelder, editor. *The Universe in Gamma-Rays*. Springer, Berlin, New York, 2001.

[6] Hirata et al. Observation of a neutrino burst from supernova sn1987a. *Physical Review Letters*, 58(14):1490–1493, April 1987.

[7] Ahmad et al. Measurement of the rate of nu(e)+d-¿p+p+e(-) interactions produced by b-8 solar neutrinos at the sudbury neutrino observatory. *Physical Review Letters*, 87(7):071301, August 2001.

[8] P. Astone, M. Bassan, P. Bonifazi, F. Bronzini, M. G. Castellano, E. Coccia, C. Cosmelli, V. Fafone, S. Frasca, E. Majorana, I. Modena, G. V. Pallottino, G. Pizzella, P. Rapagnani, F. Ricci, and M. Visco. First cooling below .1 K of the new gravitational-wave antenna Nautilus of the Rome group. *Europhysics Letters*, 16(3):231–235, 1991.

[9] Barry C. Barish and Rainer Weiss. LIGO and the detection of gravitational waves. *Physics Today*, 52(10):44–50, October 1999.

[10] B. Caron, A. Dominjo, C. Drezen, R. Flaminio, X. Grave, and Many more. The Virgo interferometer. *Classical and Quantum Gravity*, 14:1461–1469, 1997.

[11] M. Cerdonio, M. Bonaldi, D. Carlesso, E. Cavallini, S. Caruso, A. Colombo, P. Falferi, G. Fontana, P. L. Fortini, R. Mezzena, A. Ortolan, G. A. Prodi, L. Tafferello, G. Vedovato, S. Vitale, and J. P. Zendri. The ultracryogenic gravitational-wave detector AURIGA. *Classical and Quantum Gravity*, 14:1491–1494, 1997.

[12] Karsten Danzmann. LISA: laser interferometer space antenna for gravitational wave measurements. *Classical and Quantum Gravity*, 13:A247–A250, 1996.

[13] Keita Kawabe and the TAMA collaboration. Status of the TAMA project. *Classical and Quantum Gravity*, 14:1477–1480, 1997.

[14] H. Lück and the GEO600 team. The GEO600 project. *Classical and Quantum Gravity*, 14:1471–1476, 1997.

[15] Hans Ohanian and Remo Ruffini. *Gravitation and Spacetime*. W. W. Norton and Company, New York, 2nd edition, 1994.

[16] Peter R. Saulson. *Fundamentals of Interferometric Gravitational Wave Detectors*. World Scientific, Singapore, 1994.

[17] R. A. Hulse and J. H. Taylor. Discovery of a pulsar in a binary system. *Astrophysical Journal (Letters)*, 195:L51–L53, 1975.

[18] J. H. Taylor and J. M. Weisberg. A new test of general relativity — gravitational-radiation and the binary pulsar PSR-1913+16. *Astrophysical Journal*, 253:908–920, 1982.

[19] J. H. Taylor and J. M. Weisberg. Further experimental tests of relativistic gravity using the binary

pulsar PSR-1913+16. *Astrophysical Journal*, 345:434–450, October 1989.

[20] Eugene Hecht and Alfred Zajac. *Optics*. Addison-Wesley, Reading, MA, 3rd edition, 1998.

[21] R. W. P. Drever, J. L. Hall, F. V. Kowalski, J. Hough, G. M. Ford, A. J. Munley, and H. Ward. Laser phase and frequency stabilization using an optical resonator. *Applied Physics B*, 31:97–105, 1983.

[22] R. W. P. Drever, G. M. Ford, J. Hough, I. M. Kerr, A. J. Munley, J. R. Pugh, N. A. Robertson, and H. Ward. A gravity-wave detector using optical cavity sensing. In E. Schmutzer, editor, *Proceedings of the Ninth International Conference on General Relativity and Gravitation, Jena, 14–16 July 1980*, pages 265–267, Cambridge, 1983. Cambridge University Press.

[23] A. E. Siegman. *Lasers*. University Science Books, Mill Valley, CA, 1986.

[24] Eric D. Black. An introduction to Pound-Drever-Hall laser frequency stabilization. *American Journal of Physics*, 69(1):79–87, January 2001.

[25] Jordan B. Camp, H. Yamamoto, S. E. Whitcomb, and D. E. McClelland. Analysis of light noise sources in a recycled Michelson interferometer with Fabry-Perot arms. *Journal of the Optical Society of America A*, 17(1):120–128, January 2000.

[26] R. W. P. Drever. Interferometric detectors for gravitational radiation. In T. Piran and N. Deruelle, editors, *Graviational Radiation, Proceedings of the Les Houches Summer Institute, 2–21 June 1982*, Amsterdam, 1983. North-Holland.

[27] Jun Mizuno. *Comparison of optical configurations for laser-interferometric gravitational-wave detectors*. PhD thesis, Max-Planck-Institute für Quantenoptik, 85740 Garching, Bundesrepublik Deutschland, July 1995.

FIG. 1: An example of how a gravitational wave affects a compliant object. Here the wave is propagating into the page and polarized in such a way that its tidal forces are oriented along the x- and y-axes. The first figure shows the undisturbed object before the arrival of the wave, the second at a time when the tidal forces, represented by arrows, are at maximum amplitude. The third figure shows the object one-half period later, when the tidal forces have reversed. Even cataclysmic astronomical events may only produce a few cycles detectable to ground-based instruments.

FIG. 2: A basic Michelson interferometer is sensitive to just the kinds of strain a gravitational wave will produce. Incident laser light is split by a beam splitter, sent down orthogonal paths along the x- and y-axis, reflected from mirrors at the ends of these paths, and recombined back at the beam splitter. The interference between these two return beams produces a net intensity that is sensitive to differential changes in the lengths of the arms.

FIG. 3: The intensity of the light at the observation port versus the difference in arm lengths (units of λ, the wavelength of the light). Operating at point 1 maximizes the change in power for a given change in arm lengths, but it also makes the instrument sensitive to intensity noise in the light source. Operating at point 2 eliminates this problem, but, in a simple Michelson, it reduces the signal to a second order effect.

FIG. 4: An electromagnetic wave can be represented by a complex number. The length of the arrow corresponds to the amplitude of the wave, and the angle the arrow makes with the real axis corresponds to its phase.

FIG. 5: When one arm is lengthened and the other shortened slightly by a gravitational wave, the two beams in the arms acquire equal but opposite small phase shifts. The beam splitter introduces an additional 180° shift between them. The two beams add so that the net result is a small amplitude beam phase shifted 90° from the input beam.

FIG. 6: We can use lock-in detection to recover a linear signal from a dark port.

FIG. 7: The power out the dark port is the modulus squared of the sum of all the interfering beams. The two sidebands add to produce an oscillation at the modulation frequency. There are three terms in the resulting power. The signal is extracted from the term that is the product of the sidebands and the carrier.

FIG. 8: A simple mirror versus an optical delay line. In a simple mirror, light travels out a distance ℓ and reflects back, picking up a phase shift proportional to ℓ. If the mirror moves, the change in the phase shift is proportional to $\Delta\ell$. An optical path length of distance 5ℓ can be folded into a physical length ℓ with extra mirrors. If the end mirrors, three in this illustration, all move by $\Delta\ell$, the change in the phase of the reflected light is proportional to 5ℓ. We would expect a gravitational wave to move all the end mirrors together.

FIG. 9: A kind of delay line can be made with only two mirrors, if they are partially transmissive, and in this configuration it is known as a Fabry-Perot cavity. In this illustration the angle between the incident and reflected beams is greatly exaggerated. Normally this angle would be zero, *i.e.* the reflected beams travel back along the incident, and the beams bouncing back and forth between the mirrors form a standing wave. In this example, only the input (left) mirror is partially transmissive.

FIG. 10: We can substantially increase the effective arm length of a gravitational-wave detector by folding the arms. In this illustration the folding is done with Fabry-Perot cavities.

FIG. 11: The amplitude reflection coefficients for Fabry-Perot cavities are circles in the complex plane. r_i and r_o are the amplitude reflection coefficients of the input and output mirrors, respectively.

FIG. 12: On resonance, a small change in the length of a Fabry-Perot cavity dramatically changes its reflection coefficient. Plotted here is the amplitude reflection coefficient for an over-coupled Fabry-Perot cavity. Resonance is at $+1$, and the plot uses LIGO values for the mirrors [25]. 1000 points are plotted uniformly over a range in length of $\lambda/2$.

FIG. 13: To understand how a single mirror can be used to implement power recycling, we can treat the interferometer as a compound mirror and consider it the output mirror of a Fabry-Perot cavity. The recycling mirror serves as the input mirror. If the resulting recycling cavity is critically coupled, then no light is reflected back to the laser.

FIG. 14: The complete interferometric gravitational-wave detector combines Fabry-Perot arms, power recycling, and nulled lock-in detection.

FIG. 15: The shot-noise limited sensitivity for a interferometric gravitational-wave detector with $L = 4km$, $P_{in} = 10W$, $\lambda = 1.064\mu m$, $\mathcal{F}_{ac} = 130$, and $\mathcal{F}_{rc} = 100$. The frequency-dependence comes from dividing the shot noise in the photodiode by the response of the interferometer.

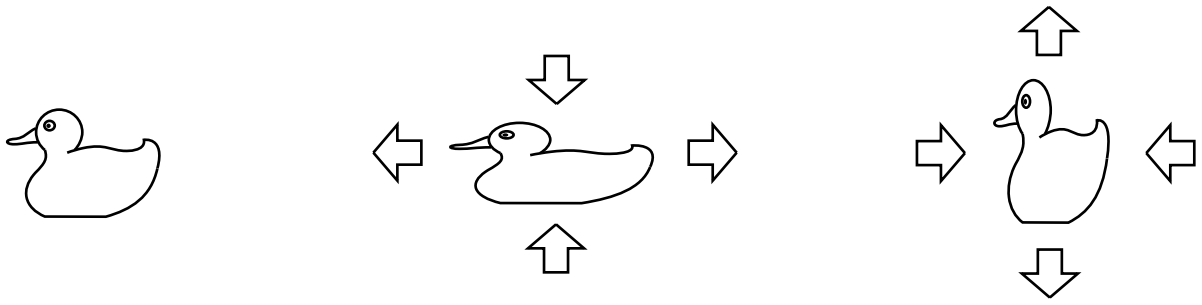

FIG 1 BLACK AM.J. PHYS

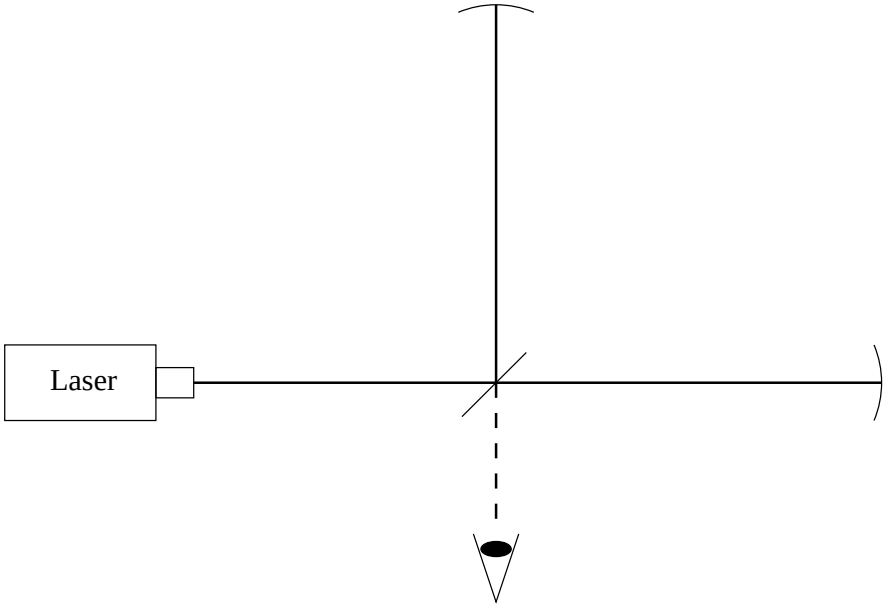

FIG 2 BLACK AM.J. PHYS

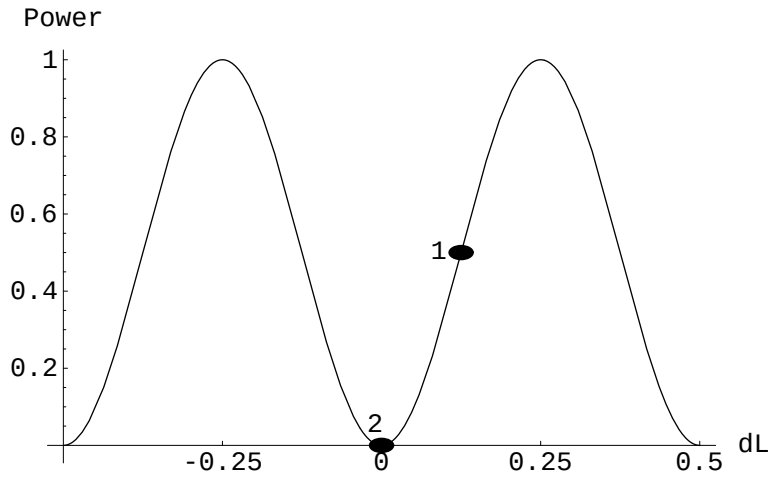

FIG 3 BLACK AM.J. PHYS

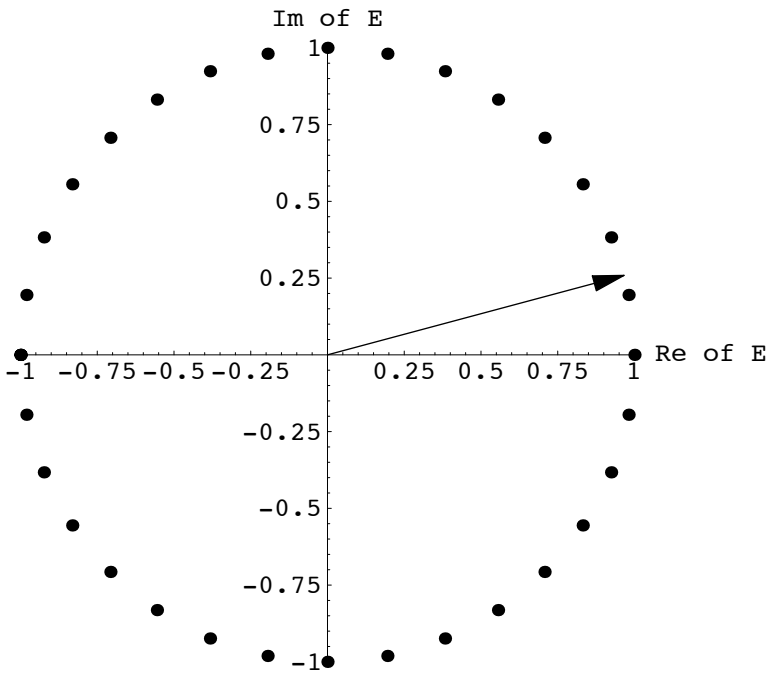

FIG. 4 BLACK AM. J. PHYS.

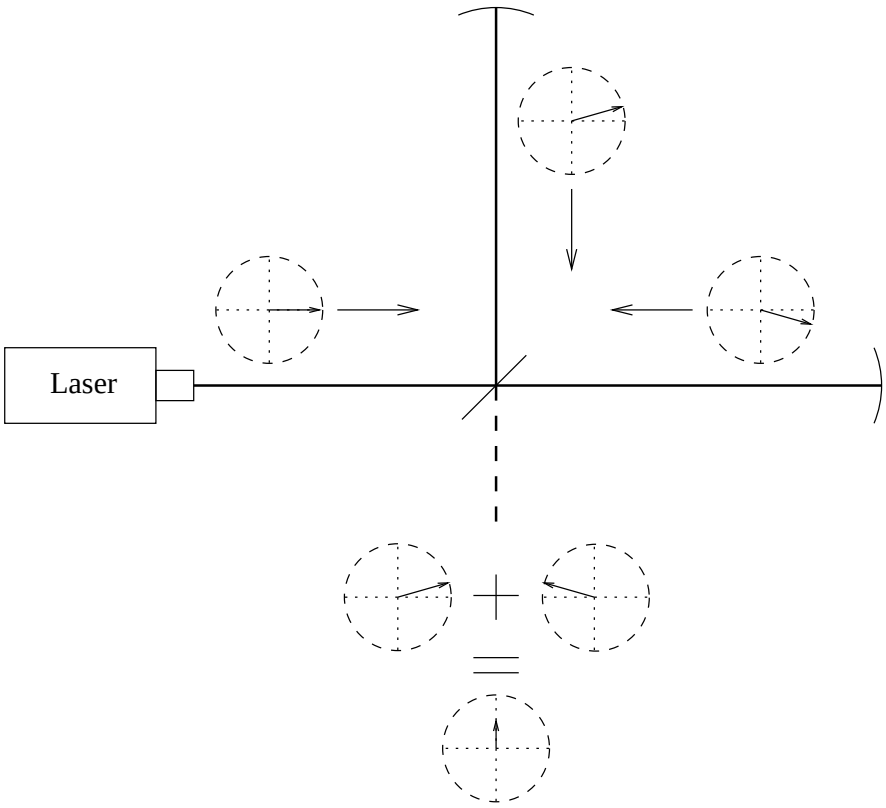

FIG 5 BLACK AM.J. PHYS

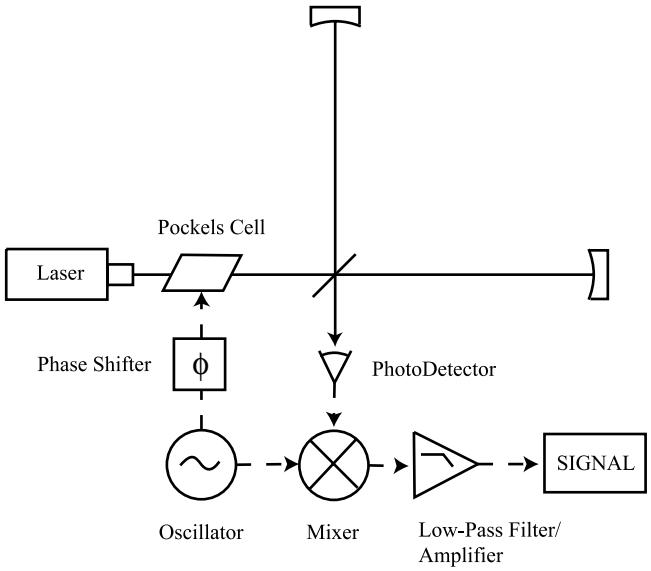

FIG 6 BLACK AM.J. PHYS

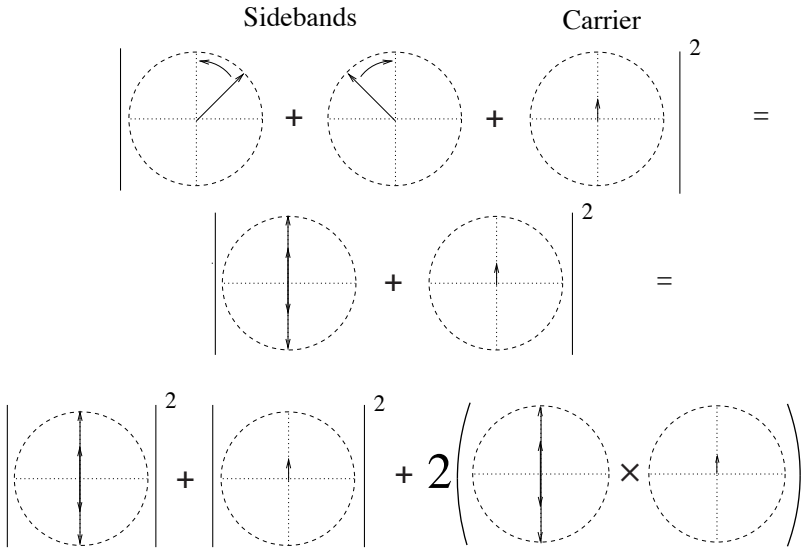

FIG. 7 BLACK AM. J. PHYS.

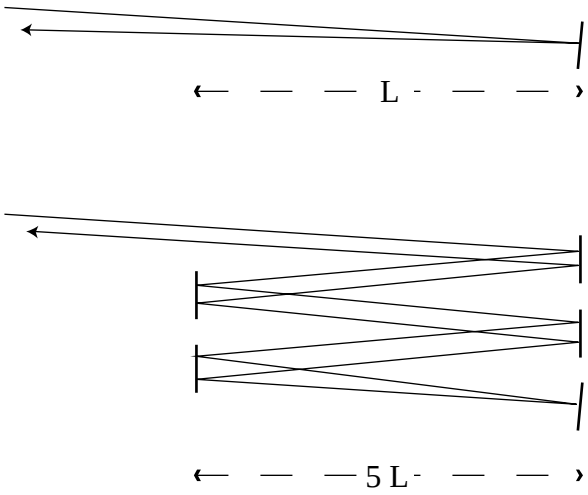

FIG 8 BLACK AM.J. PHYS

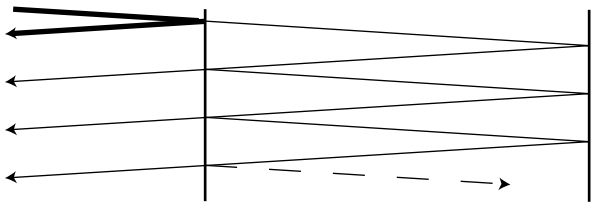

FIG 9 BLACK AM.J. PHYS

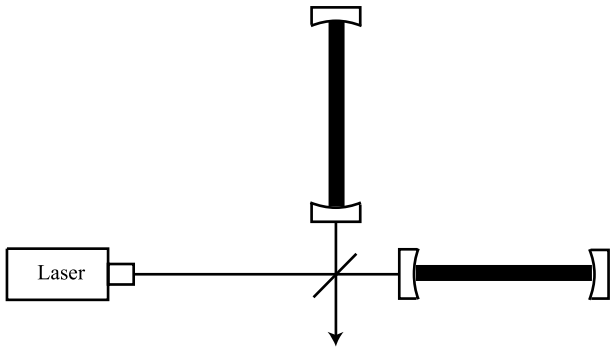

FIG 10 BLACK AM.J. PHYS

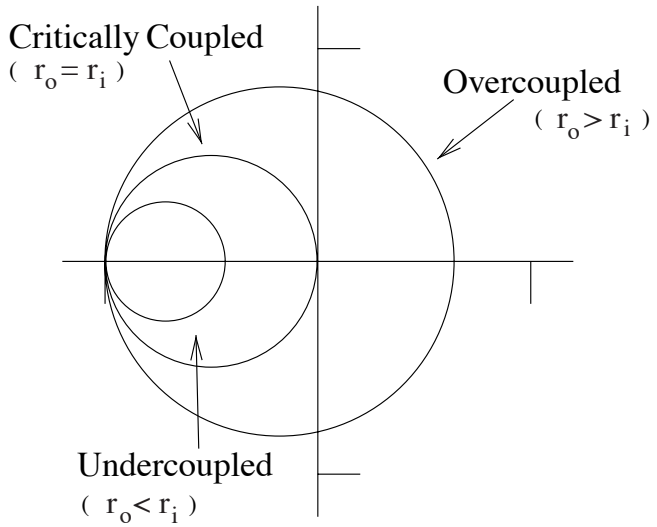

FIG. 11 BLACK AM. J. PHYS.

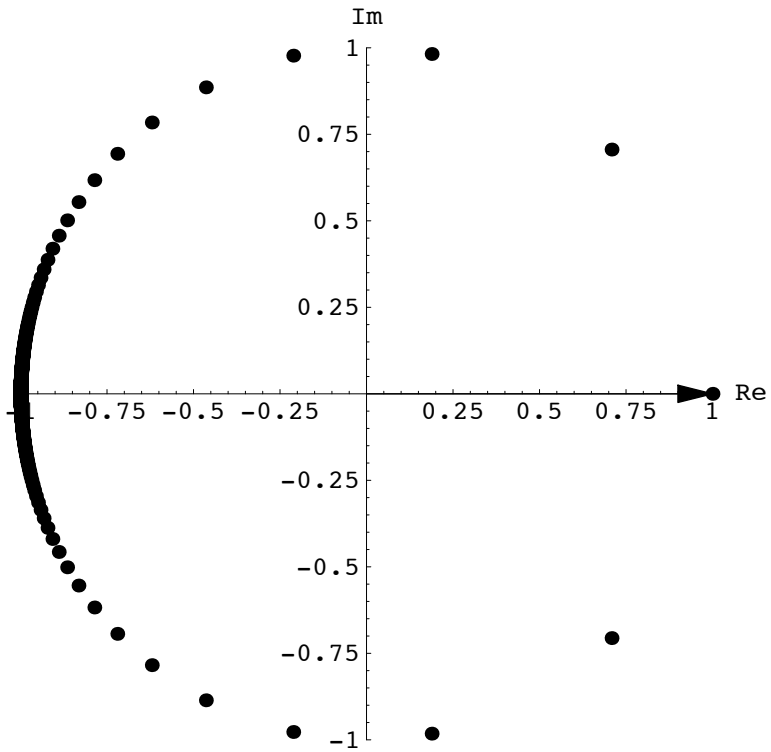

FIG. 12 BLACK AM. J. PHYS.

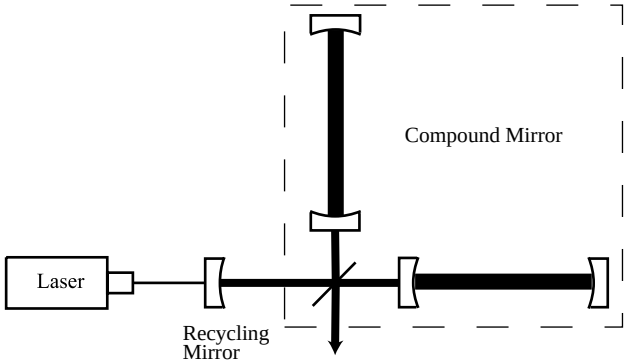

FIG 13 BLACK AM.J. PHYS

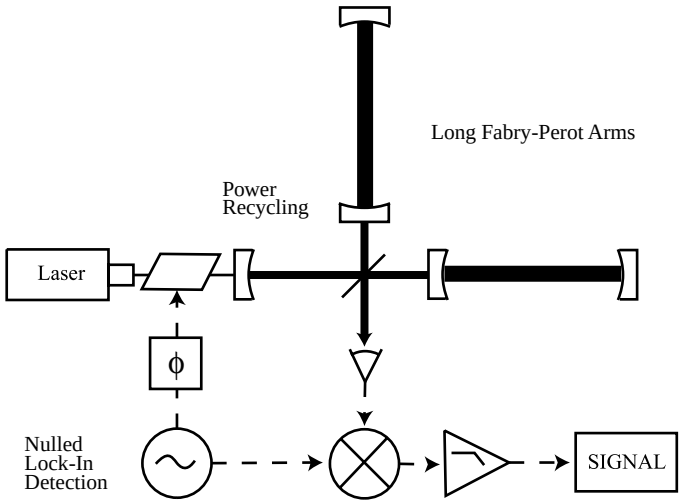

FIG 14 BLACK AM.J. PHYS

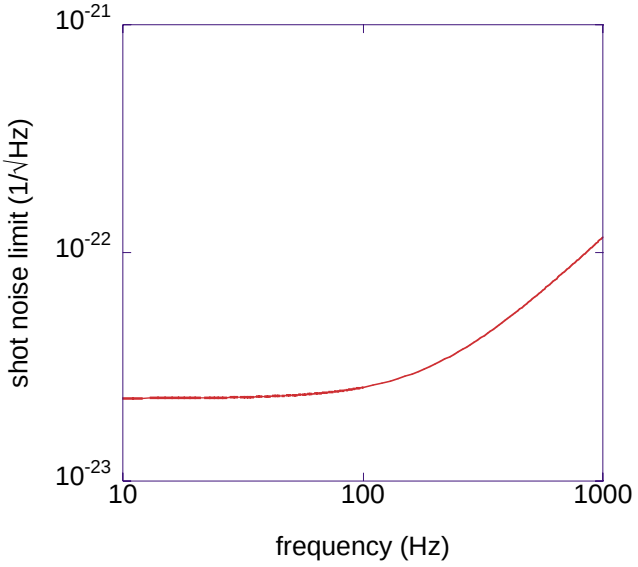

FIG 15 BLACK AM.J. PHYS